

Transport resistance strikes back: unveiling its impact on fill factor losses in organic solar cells

Maria Saladina^{1,*} and Carsten Deibel^{1,†}

¹*Institut für Physik, Technische Universität Chemnitz, 09126 Chemnitz, Germany*

The fill factor (FF) is a critical parameter for solar cell efficiency, yet its analytical description is challenging due to the interplay between recombination and charge extraction processes. An often overlooked yet significant factor contributing to FF losses, beyond recombination, is the influence of charge transport. In most state-of-the-art organic solar cells, the primary limitation of the FF arises not from recombination but rather from low conductivity, highlighting the need for refined models to predict the FF accurately. Here, we extend the analytical model for transport resistance to a more general case. Drawing from a large set of experimental current–voltage and light intensity-dependent open-circuit voltage data, we systematically incorporate crucial details previously omitted in the model. Consequently, we introduce a straightforward set of equations to predict the FF of a solar cell, enabling the differentiation of losses attributed to recombination and transport resistance. Our study provides valuable insights into strategies for mitigating FF losses based on the experimentally validated analytical model, guiding the development of more efficient solar cell designs and optimization strategies.

Keywords: organic solar cells; fill factor; transport resistance; ideality factor

1. Introduction

Lately we have witnessed remarkable progress in enhancing the efficiency of organic solar cells (OSCs),^{1,2} paving the way for financially viable upscaling. Therefore, the research community is shifting its attention towards the critical aspect of stability.^{3,4} Even state-of-the-art solar cells can experience parameter losses due to degradation.^{5,6} Recent research has revealed that thermal degradation is a contributing factor that leads to a reduction in the FF of OSCs.⁷ This reduction is mainly attributed to increased trapping of charge carriers and transport resistance. The latter scales linearly with active layer thickness,⁸ making it particularly relevant for commercial-scale manufacturing.

Among the FF loss mechanisms shown in Figure 1, transport resistance has been overlooked compared to the more extensively studied geminate and nongeminate recombination.^{9–12} Several studies predicted that, besides recombination, the reduction in FF of OSCs was attributed to slow charge transport.^{13,14} In 2014, Schiefer et al. laid down a theoretical framework to describe transport resistance in OSCs.⁸ Similar work was done before on comparable p-i-n junctions.¹⁵ Utilizing this framework, they determined intrinsic charge carrier density within the active layer by comparing the experimental current–voltage ($j(V)$) curve to its resistance-free counterpart. The latter was approximated by the $\text{suns-}V_{oc}$ curve, i.e. the open-circuit voltage of a solar cell measured over several orders of magnitude of light intensities, downshifted by the short-circuit current density j_{sc} . Mäkel and MacKenzie revisited this method for

determining charge carrier mobility, applying it to transient photovoltage and photocurrent techniques.¹⁶ Comparison with drift-diffusion simulations demonstrated the method’s accuracy in extracting effective mobility.

Further significant contributions to the model of transport resistance were based on drift-diffusion simulations. Bartesaghi et al. observed, through both simulation and experiment, that the FF of OSCs is governed by the interplay between charge carrier recombination and extraction.¹⁷ Würfel et al. further demonstrated that the FF in OSCs is limited by slow transport, leading to the accumulation of charge carriers within the device.¹⁸ They highlighted a substantial difference between the applied voltage considered in the diode equation and the actual quasi-Fermi level splitting (QFLS), leading to the gradient of the QFL in the active layer. Neher et al. unified two seemingly different approaches,¹⁹ elucidating how the slope of the $j(V)$ curve around V_{oc} influences the FF

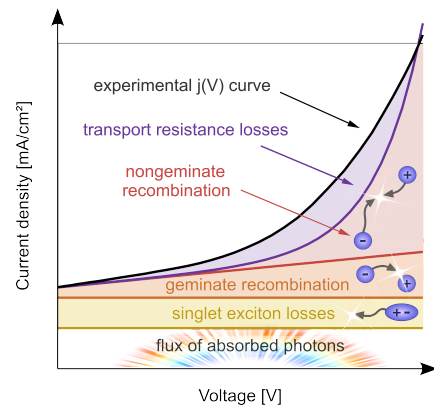


Figure 1. Schematic representation of the impact of main loss mechanisms on the $j(V)$ -curve of OSC.

* email: maria.saladina@physik.tu-chemnitz.de

† email: deibel@physik.tu-chemnitz.de

and alters the apparent ideality factor in the diode equation. The slope was parameterized by the figure of merit α , a measure of transport-induced series resistance near V_{oc} . A figure of merit reciprocal to α , the $\mu\tau$ -product, was related to the FF by Kaienburg et al.,²⁰ and by Xiao et al.²¹ with focus on the impact of tail state traps.

The validity of these predictions is now being substantiated by experimental data. Tokmoldin et al. assessed the $\mu\tau$ -product in various organic fullerene and state-of-the-art nonfullerene-acceptor (NFA) solar cells.²² While the solar cell performance was not limited at j_{sc} , FF losses were influenced by the transport resistance near V_{oc} . Yang et al. observed improved charge carrier collection efficiency in doped NFA OSCs, positively affecting both FF and device stability.²³ A link between transport resistance and stability was established in our study on thermal degradation in PM6:Y6 solar cells.⁷ Employing the suns- V_{oc} method, we identified transport resistance as the primary factor driving the decrease in photovoltaic performance after 96 hours of thermal stress at 85 °C. Experimental observations supported by drift-diffusion simulations indicated increased defect formation in the active layer as the likely source of elevated transport resistance. The influence of transport resistance on FF extends beyond OSCs,^{24,25} for systems that exhibit significantly lower mobility compared to crystalline semiconductors.

Despite evidence of a detrimental impact on the solar cell performance, experimental measurements of transport resistance are scarce, leaving the models largely untested. While transport resistance models provide qualitative predictions for FF , they have not been sufficiently refined to align with experimental data. Often these models assume ideal transport and recombination, neglecting trap states entirely or treating their distribution as Gaussian. In this paper, we refine the analytical model for transport resistance based on experimental data. We extend the diode equation to accommodate both limited extraction and recombination, allowing for non-unity ideality factors. We establish a precise method for evaluating the effective conductivity at open circuit, through straightforward measurements of $j(V)$ and the light intensity-dependent V_{oc} of a solar cell. Our model allows to understand the contributions of the two charge carrier types to recombination and transport, and to predict the FF limitations at both open circuit and the maximum power point (MPP). Based on the experimentally verified analytical model, our study provides insights into approaches aimed at minimizing FF losses.

2. Results and Discussion

2.1. The diode equation

Transport resistance is an internal resistance within the active layer resulting from the relatively slow move-

ment of charge carriers, effectively acting as an internal series resistance. As shown in Figure 2(a), we evaluate this resistance by comparing a pseudo- $j(V)$ curve, encompassing recombination losses, with the experimental $j(V)$ curve under illumination, which encompasses both recombination and transport resistance losses.

Analytically, both curves can be characterized using the diode equation. The pseudo- $j(V)$ curve depends on the implied voltage V_{imp} , i.e., the QFLS divided by the elementary charge e , and accounts solely for recombination losses (both geminate and nongeminate), excluding transport resistance.^{18,19,26}

$$j(V_{imp}) = j_{gen} \left[\exp \left(\frac{e(V_{imp} - V_{oc})}{n_{id}k_B T} \right) - 1 \right], \quad (1)$$

where j_{gen} stands for the generation current density, the sum of the dark saturation current density j_0 and the photocurrent density j_{photo} , n_{id} stands for the recombination ideality factor, k_B the Boltzmann constant, and T the temperature. From the latter equation it follows that one can obtain the pseudo- $j(V)$ curves experimentally from the suns- V_{oc} measurements using the superposition principle. In this context, V_{imp} represents the open-circuit voltage measured under a specific light intensity Φ . We constructed $j(V_{imp})$ by shifting a suns- V_{oc} curve downward by j_{gen} , a value estimated from the current density at -0.5 V for a given temperature and light intensity (see Figure S1).

For infinite charge carrier mobility, an externally applied voltage V_{ext} equals V_{imp} , the voltage that charge carriers feel within the device, and the quasi-Fermi levels in the bulk are flat. However, in reality, charge carrier mobility is finite. Slow charge carrier transport leads to a tilting of the quasi-Fermi levels and gives rise to a discrepancy between V_{ext} and V_{imp} , as shown in Figure 2(b) for PM6:Y6. This discrepancy is what we refer to as the voltage loss due to transport resistance, defined as^{8,19}

$$\Delta V_{tr} = j \cdot \frac{L}{\sigma} = \frac{\nabla E_F}{e} \cdot L. \quad (2)$$

Here j is the current density, L the active layer thickness, σ the conductivity, and ∇E_F the gradient of the quasi-Fermi levels. We determined ΔV_{tr} from the experimental data as $\Delta V_{tr}(j) = V_{ext}(j) - V_{imp}(j) - jR_{ext}$, i.e. the difference between the experimental $j(V)$ and the downshifted suns- V_{oc} curve at the same current density, while also factoring in R_{ext} , the series resistance of the circuit. The latter was estimated from fitting dV_{ext}/dj at high forward bias, where transport resistance is negligible.

The experimental $j(V)$ curve under illumination is described by the diode equation similar to Eq. (1), but it is expressed in terms of V_{ext} ,

$$\begin{aligned} j(V_{ext}) &= j_{gen} \left[\exp \left(\frac{e(V_{ext} - \Delta V_{tr} - jR_{ext} - V_{oc})}{n_{id}k_B T} \right) - 1 \right] \\ &= j_{gen} \left[\exp \left(\frac{e(V_{ext} - V_{oc})}{n_{app}k_B T} \right) - 1 \right]. \end{aligned} \quad (3)$$

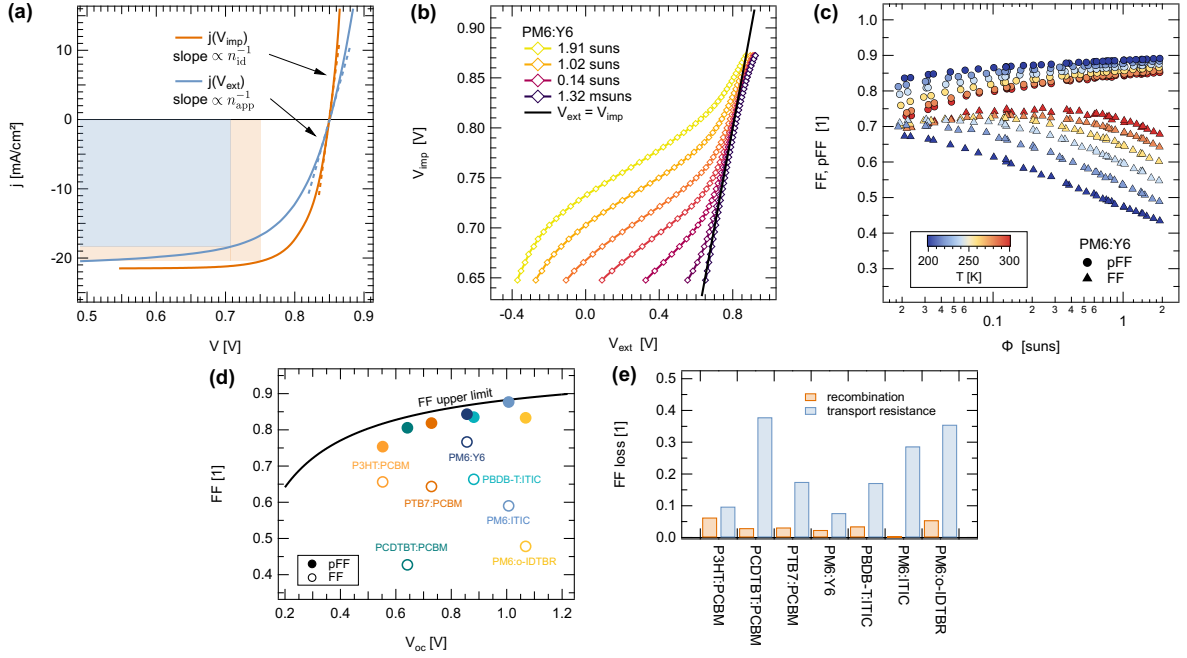


Figure 2. (a) A pseudo- $j(V)$ curve, $j(V_{\text{imp}})$, contains recombination losses, while an experimental $j(V)$ curve, $j(V_{\text{ext}})$, incorporates additional losses due to transport resistance. Their slopes at V_{oc} are inversely proportional to n_{id} and n_{app} , respectively. The shaded areas correspond to the output power at their respective MPPs. (b) The difference between the implied voltage V_{imp} and the externally applied voltage V_{ext} arises due to transport resistance, which is more pronounced at higher light intensities. (c) pFF and FF of a PM6:Y6 solar cell as a function of light intensity Φ . While pFF increases with Φ owing to reduced disorder, FF decreases due to higher transport resistance. (d) Comparison of pFF and FF in solar cells based on different donor-acceptor blends. The solid line indicates the FF upper limit (solid line) was determined using Eq. (8) with $a = 0.72$ and $n_{\text{app}} = 1$. (e) FF losses attributed to recombination and transport resistance, with the latter emerging as the primary loss across all donor-acceptor systems.

Here n_{app} stands for the apparent ideality factor, which takes into account the combined influence of recombination, transport and external series resistance.

At a given current density, Eqs. (1) and (3) can be set equal, and the apparent ideality factor is expressed as $n_{\text{app}} = n_{\text{id}} + \beta$, with parameter β defined as

$$\beta(V_{\text{ext}}) = n_{\text{id}} \cdot \frac{\Delta V_{\text{tr}}}{V_{\text{imp}} - V_{\text{oc}}}. \quad (4)$$

The above equation is valid with the assumption that the influence of R_{ext} in the fourth quadrant of the $j(V_{\text{ext}})$ curve is much smaller than that of the transport resistance.

Both $j(V)$ curves, given by Eqs. (1) and (3), can be evaluated in terms of their fill factor, a key factor in determining the overall efficiency of a solar cell. Figure 2(c) presents a comparison of the fill factors obtained from $j(V_{\text{imp}})$, determined by the suns- V_{oc} method, and $j(V_{\text{ext}})$ for a PM6:Y6 solar cell, which were measured over a broad range of temperatures and light intensities. The pseudo-fill factor, denoted as pFF , characterises the fill factor of a solar cell when transport resistance is absent, and represents its upper limit.^{7,25,27} It tends to improve with higher light intensity, which we attribute to reduced

energetic disorder as the QFLS increases.²⁸ In contrast to pFF , the fill factor of an experimental $j(V)$ curve tends to decrease with increasing light intensity, as the transport resistance becomes more significant. Certainly, in the case of PM6:Y6 solar cells, the losses due to transport resistance outweigh the losses caused by recombination. As we demonstrate in Figures 2(d) and 2(e), this trend is not unique to PM6:Y6 but can also be observed in various other OSCs, where transport resistance tends to be the primary contributor to performance losses under operating conditions.

The ideality factor changes the slope of the $j(V)$ curve, and thus affects the FF by impacting the ability of the solar cell to operate at its MPP. A less steep slope leads to a lower FF , indicating reduced efficiency in converting light into electrical power. The resistance-free pseudo- $j(V)$ curve in Figure 2(a) is solely affected by recombination, and its slope is inversely proportional to n_{id} , as follows from Eq. (1). The ideality factor of the experimental $j(V)$ curve, n_{app} , is increased by an additional term containing both transport and external series resistance. This alteration results in a shallower slope and causes the operating point to deviate from the theoretically achievable MPP, leading to a lower FF .

2.2. The open circuit. The figure of merit α .

Neher et al. showed that near open circuit $n_{\text{app}} = 1 + \alpha$, where $n_{\text{id}} = 1$ and α was the figure of merit for OSCs with transport-limited photocurrents.¹⁹ In most cases n_{id} differs from unity, and we find that the apparent ideality factor becomes $n_{\text{id}} + \alpha$ (for derivation please refer to Section S3 in Supporting Information). This correction becomes important for the values of α comparable to n_{id} . Very generally, α is a measure of the competition between recombination and conductivity at open circuit conditions

$$\alpha = \frac{eL}{k_B T} \cdot \frac{j_{\text{gen}}}{\sigma_{V_{\text{oc}}}}, \quad (5)$$

where recombination current density equals j_{gen} at V_{oc} . The figure of merit α can be determined experimentally by using just two data sets – the suns- V_{oc} and the $j(V)$ of a solar cell, with j_{gen} estimated from $j(V)$ at a sufficiently high reverse bias.

Conductivity can generally be determined from Eq. (2), although it leads to a discontinuity at V_{oc} , where $\Delta V_{\text{tr}} = 0$.^{8,16} We overcome this obstacle in a simple way using a derivative. As both j and σ change as we move along the $j(V)$ curve, the derivative $d\Delta V_{\text{tr}}/dj$ given by Eq. (S1) has two terms. At V_{oc} , however, only one of them is non-zero, yielding

$$\sigma_{V_{\text{oc}}} = L \cdot \left(\frac{d\Delta V_{\text{tr}}}{dj} \Big|_{j=0} \right)^{-1}. \quad (6)$$

The condition of equal electron and hole current densities in the bulk implies, when applied to Eq. (2), that $\sigma_n \cdot \Delta V_{\text{tr},n} = \sigma_p \cdot \Delta V_{\text{tr},p}$. If the conductivity of one charge carrier type is lower compared to the other, then ΔV_{tr} , represented by the gradient of its Fermi level, is inevitably higher. As a result, in cases of imbalanced conductivity, the FF is limited by the slower-moving charge carrier. This also means that the effective conductivity extracted by our method, Eq. (6), is a harmonic mean of the electron and hole conductivity.

The conductivity, determined from the slope of ΔV_{tr} according to Eq. (6), is depicted in Figure 3(a). As expected, it increases with higher light intensity and temperature, following the rise in charge carrier density n , as $\sigma = e\mu_{\text{eff}} \cdot n$. The effective mobility μ_{eff} generally improves as the share of mobile charge carriers increases. Intuitively, we anticipate an improvement in the FF with increased light intensity, as the traps get filled and transport becomes better (at least this is true for the exponential distribution of trap states). However, contrary to this expectation, the data in Figure 2(c) shows that the FF of the PM6:Y6 solar cell decreases with higher illumination. The figure of merit α can provide an explanation for this observation. As σ in Eq. (5) increases, so does j_{gen} . Both of these competing processes depend on light intensity, yet j_{gen} depends on it more strongly

than σ , leading to an increase in α and an overall lower fill factor.

Disorder. Figure 3(b) presents the α values for a PM6:Y6 solar cell over a wide range of temperatures and light intensities, which were calculated from the experimental data using Eq. (5). To understand the exact parameters affecting α , we are interested in the slopes. The data shows that $\alpha \propto \sqrt{\Phi}$, deviating at lower illumination intensities. From the definition of α , it is evident that it is related to Φ through the light intensity dependence of both j_{gen} and $\sigma_{V_{\text{oc}}}$. When the net current is zero, the charge carrier generation and recombination rates are equal and the light intensity is related to V_{oc} as $\ln \Phi \propto eV_{\text{oc}}/n_{\text{id}}k_B T$. In the models α is typically assumed to be proportional to $\sqrt{\Phi}$, because j_{gen} and $\sigma_{V_{\text{oc}}}$ in the simplest case (considering a Gaussian distribution of tail states, or ignoring them entirely) scale with ideality factors of 1 and 2, respectively. However, this assumption is not accurate for the general case.^{29–31}

Both j_{gen} and $\sigma_{V_{\text{oc}}}$ have additional voltage dependence, and can generally be defined at V_{oc} as $j_{\text{gen}} = j_{00} \exp[-(E_g - eV_{\text{oc}})/n_{\text{id}}k_B T]$, and $\sigma_{V_{\text{oc}}} = \sigma_{00} \exp[-(E_g - eV_{\text{oc}})/n_{\sigma}k_B T]$, with j_{00} and σ_{00} denoting temperature-independent prefactors. The recombination ideality factor of PM6:Y6 in Figure 3(c) is unity only in the small range of light intensities close to 1 sun. Similarly, σ has a transport ideality factor $n_{\sigma} \neq 2$ for most of the range. Both ideality factors originate from the trapping and subsequent release of charge carriers within the active layer, and the precise analytical models depend on the densities of localized states.^{28,31,32} To address this important detail, we have incorporated ideality factors into the analytical model of α . This leads to

$$\alpha = \frac{eL}{k_B T} \cdot \frac{j_{00}}{\sigma_{00}} \cdot \exp \left[-\frac{E_g - eV_{\text{oc}}}{k_B T} \left(\frac{1}{n_{\text{id}}} - \frac{1}{n_{\sigma}} \right) \right] \propto \Phi^{1 - \frac{n_{\text{id}}}{n_{\sigma}}}. \quad (7)$$

The slope in Figure 3(b) corresponds to $1 - n_{\text{id}}/n_{\sigma}$, as can be seen from Eq. (7). The value of this slope depends on which type of charge carrier, electrons or holes, dominates the transport and recombination processes. We have previously demonstrated that the density of states (DOS) for electrons and holes in PM6:Y6 can be accurately described as a combination of Gaussian and power-law distributions, where the latter can be approximated by an exponential function at a given QFLS.²⁸ Recombination in PM6:Y6 is primarily driven by mobile charge carriers from the Gaussian DOS interacting with charge carriers trapped in the power-law DOS.

When transport resistance is governed by the same mobile charge carrier, the application of the multiple trapping and release model results in $n_{\text{id}}/n_{\sigma} = 1/2$ (see Supporting Information, Section S4), meaning that α scales with a square root of light intensity. On the other hand, if transport is limited by the mobile charge carriers from the power-law DOS, then $n_{\text{id}}/n_{\sigma} = n_{\text{id}} - 1/2$, and α scales with a power of light intensity. This power is equal to $1/2$

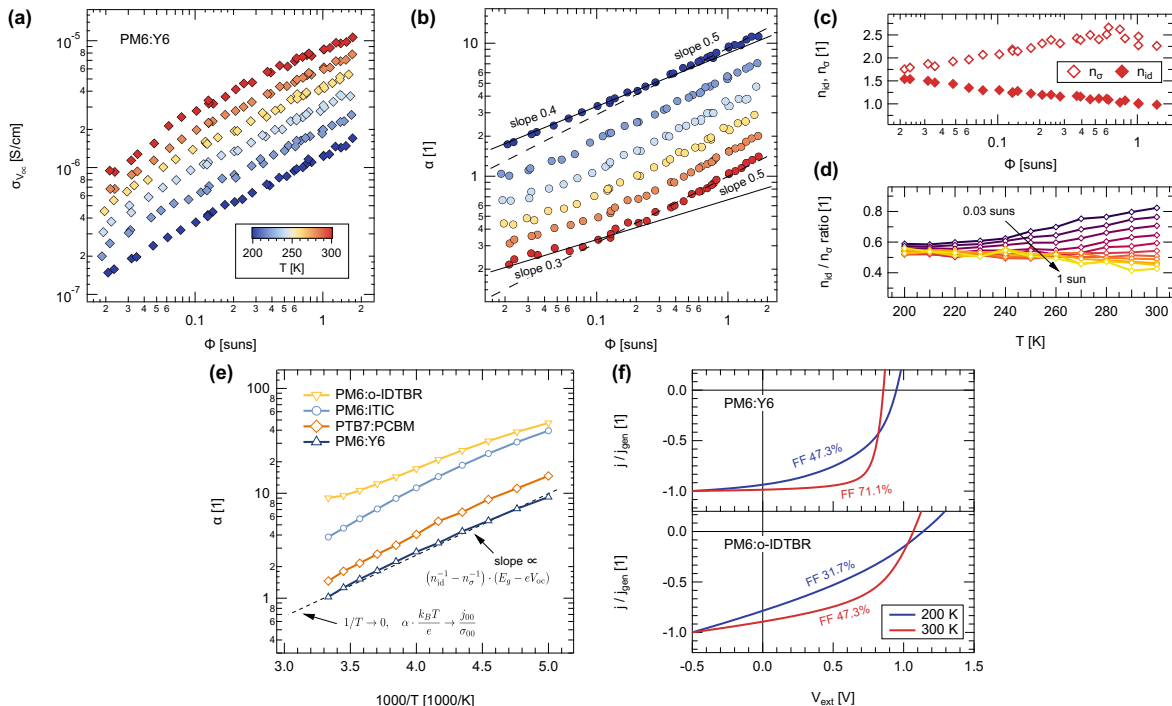


Figure 3. (a) $\sigma_{V_{oc}}$ determined from the slope of ΔV_{tr} according to Eq. (6). Its increase with light intensity does not have a positive impact on the FF in Figure 2(c). (b) Light intensity dependence of α for PM6:Y6. The slope at low Φ deviates from the commonly assumed 1/2. (c) The ideality factors for recombination (n_{id}) and transport (n_{tr}) at 300 K. Deviations from the values of $n_{id} = 1$ and $n_{tr} = 2$, commonly assumed in the models, necessitate the incorporation of these factors into the analytical expression for α . (d) The ratio of the ideality factors is ≈ 0.5 at higher Φ but increases at lower Φ , explaining the slope of $\alpha(\Phi)$. (e) Temperature dependence of α for different material systems. (f) Comparison of the $j(V)$ curves at 200 K and 300 K. Higher α of PM6:o-IDTBR at 200 K severely impacts the FF , leading to a transport-controlled $j(V)$ -curve.

only if $n_{id} = 1$, in other cases it is lower than 0.5. The slope in Figure 3(b) is < 0.5 at lower QFLS, aligning precisely with the ratio of the ideality factors depicted in Figure 3(d). This alignment indicates that transport in PM6:Y6 is limited by mobile charge carriers from the power-law DOS. At a higher QFLS the slope is 0.5, but the dominance of charge carriers is unclear, as n_{id} is close to unity. In general, a lower ratio of n_{id} to n_{tr} leads to a decrease of α and an improvement of the fill factor.

Temperature dependence. Figure 3(e) illustrates the α values of various solar cells as a function of temperature under 1 sun illumination intensity. The active layers of the devices were composed of PM6:Y6, PM6:ITIC, PM6:o-IDTBR and PTB7:PCBM blends. For detailed information about the fabrication of these solar cells, please refer to the Section S1, Supporting Information. Although one might intuitively expect PM6:o-IDTBR to exhibit a lower α value compared to other solar cells due to its higher effective bandgap, the data contradicts this assumption.³³ At 300 K, it demonstrates the highest α among the four, owing to a compensation effect from a remarkably low value of $n_{id}^{-1} - n_{tr}^{-1} = 0.27$ (whereas the values for PM6:Y6 and PM6:ITIC are above 0.5). Additionally, the temperature-independent prefactor j_{00}/σ_{00}

also exhibits the highest value, as inferred from extrapolating the data to $1/T = 0$.

At 300K, $\alpha \approx 1$ for PM6:Y6, yet the fill factor in Figure 3(f) falls well below the pFF limit of 84 %. PM6:Y6 at 200 K and PM6:o-IDTBR at 300 K both exhibit $\alpha \approx 9$, coinciding with identical fill factors at these temperatures. At 200 K, the value of α for PM6:o-IDTBR surges by a factor of 5, while the fill factor drops to a mere 31.7 %. Assuming the generation rate of charge carriers remains temperature-independent (or weakly temperature-dependent), the temperature dependence of α is primarily dictated by σ . As temperature rises, the share of mobile charge carriers increases, facilitated by their easier thermal release from shallow traps. Consequently, higher conductivity at the same generation rate lowers the α value and enhances the FF .

2.3. The maximum power point

Let us now turn our attention to the fill factor and examine how effectively α accounts for its behaviour. The analytical expression for the FF requires the definition of the normalized voltage v_{ext} .²⁷ Here, it is de-

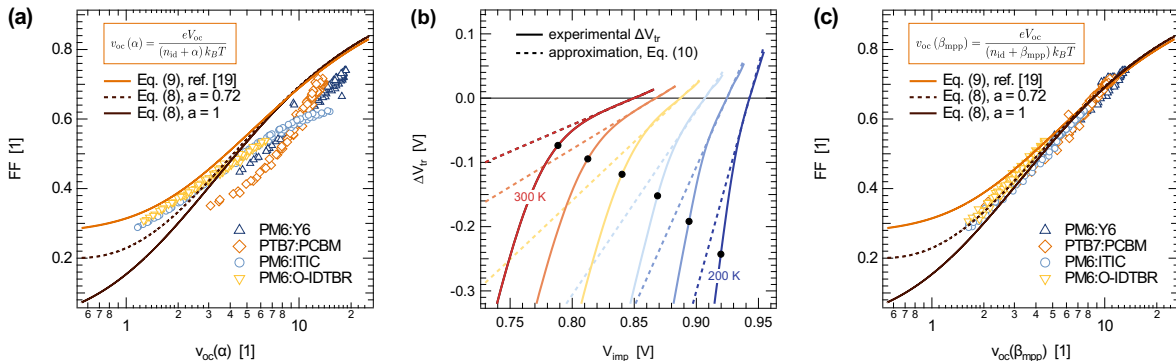


Figure 4. (a) The relationship between FF and $v_{oc}(\alpha)$ varies depending on the material system. (b) Comparison between experimental and calculated ΔV_{tr} for PM6:Y6. The approximation using α (Eq. (10), dashed lines) underestimates the experimental ΔV_{tr} (solid lines) at MPP (indicated by black dots). (c) FF vs v_{oc} fitted using Eq. (8) with $a = 0.72$. The fit applies universally to various solar cells when v_{oc} is evaluated using β_{mpp} , which accurately considers the voltage dependence of transport resistance.

defined as V_{ext} divided by the thermal voltage $k_B T/e$ and n_{app} . One finds, that at MPP, the normalized voltage v_{mpp} can be approximated³⁴ using the normalized open-circuit voltage v_{oc} , as $v_{mpp} \approx v_{oc} - \ln(v_{oc} + 1)$ (for details see Section S6 in Supporting Information). By using this approximation, the fill factor can be related to v_{oc} via^{27,34–36}

$$FF = \frac{v_{oc} - \ln(v_{oc} + a)}{v_{oc} + 1}. \quad (8)$$

This equation was used for inorganic solar cells to estimate an upper limit of the FF , assuming infinite shunt and zero series resistance.^{27,35} To align better with experimental results, $a = 1$ under the logarithm was empirically replaced by $a = 0.72$.²⁷

When applied to OSCs,¹⁹ a large set of simulated FF vs α showed deviations from Eq. (8). A new fit equation was therefore proposed,

$$FF = \frac{v_{oc} - \ln(0.66v_{oc}^{1.2} + 0.79)}{v_{oc} + 1}, \quad (9)$$

with v_{oc} calculated using $n_{app} = n_{id} + \alpha$, where n_{id} was assumed to be unity. This relation was expected to hold across different material systems characterized by low charge carrier mobility.

To confirm the validity of Eq. (9), we have assessed the parameter α experimentally for wide range of temperatures and illumination intensities for four OSCs. Figure S2 demonstrates experimental confirmation of the predicted relationship between the FF and the parameter α .^{17,19} This relationship indicates the direction for any given system for higher illumination intensity and effective disorder, for example by lowering the temperature (c.f. Figures 3(b) and (e)) or through degradation within the device.

To relate α to the fill factor we calculate the normalized open-circuit voltage using $n_{app} = n_{id} + \alpha$, as originally suggested,¹⁹ but use the measured values of n_{id}

instead of assuming $n_{id} = 1$. The results are shown in Figure 4(a). For a particular system, we observe a consistent data alignment across the measured range of temperatures and light intensities. In qualitative terms, the model is highly effective. When examining the relation between the experimental FF and α across various solar cells, we observe that the dependence of FF on α varies for each material system. Consequently, the fitting equation for $FF(\alpha)$ is unique to each system, a result that was unexpected.

The next aspect to unravel is why α can not accurately predict the FF of all solar cells using a single equation. As already mentioned, $n_{id} + \alpha$ determines the slope of the $j(V_{ext})$ curve at the open circuit conditions, while the pseudo- $j(V)$ curve, $j(V_{imp})$, has the slope corresponding to n_{id} . By setting the current density of both $j(V)$ curves in Eqs. (1) and (3) equal, we find – extending the work by Neher et al. – that around V_{oc}

$$\Delta V_{tr} \approx \frac{\alpha}{n_{id}} (V_{imp} - V_{oc}). \quad (10)$$

The parameter α remains constant at a given temperature and light intensity, in other words it does not depend on implied and external voltage. If α were capable of consistently predicting ΔV_{tr} across all voltages in the $j(V)$ curve, then the change in V_{imp} should be sufficient to account for the change in ΔV_{tr} .

The relationship given by Eq. (10) is depicted in Figure 4(b) for a PM6:Y6 solar cell, alongside the measured ΔV_{tr} . In close proximity to V_{oc} , the approximation provided by Eq. (10) demonstrates excellent agreement with the data. However, away from V_{oc} the discrepancy between the experimental data and the model becomes more evident. Particularly, at MPP (marked by black dots), the model significantly underestimates ΔV_{tr} . Hence, an accurate prediction of the FF requires an additional factor that accounts for the voltage-dependence of the transport resistance, as provided by Eq. (S3). The

apparent ideality factor incorporated into the normalized voltage must accurately reflect the influence of the transport resistance, thus β must be used instead of α .

In Figure 4(c), we show that Eq. (8) is sufficient without alterations to describe the fill factor of all investigated solar cells in the temperature range of 200 to 300 K. For the normalized open-circuit voltage, the apparent ideality factor $n_{\text{app}} = n_{\text{id}} + \beta$ is employed, where parameter β is defined by Eq. (4) and is evaluated at MPP. Remarkably, Eq. (8) with $a = 0.72$ universally predicts the fill factor across values ranging from as low as 29 % up to 75 %. In Figure S3(a) it is demonstrated to work reasonably well for fill factors at the upper limit, describing the pseudo-fill factor in PTB7:PCBM. Interestingly, when Eq. (8) is employed with $a = 1$, it fits the fill factors as a function of normalized voltage when the former is evaluated using j_{gen} instead of j_{sc} (c.f. Figure S3(b)). This adjustment aligns with the derivation of Eq. (8), which requires the use of j_{gen} in the diode equation.

Since the voltage at MPP can be linked to V_{oc} , it allows the adoption of several useful simplifications when evaluating solar cell parameters. At MPP β can be predicted just from the values of α , V_{oc} and the ideality factors by iteration,

$$\beta_{\text{mpp}} = \alpha \cdot \frac{v_{\text{oc}} \cdot (v_{\text{oc}} + 1)^{\frac{n_{\text{id}}}{n_{\sigma}} - 1}}{\ln(v_{\text{oc}} + 1)}, \quad (11)$$

where v_{oc} depends on β_{mpp} as $eV_{\text{oc}} / (n_{\text{id}} + \beta_{\text{mpp}}) k_B T$ (for detailed derivation refer to Section S7, Supporting Information). This fast converging iterative scheme agrees reasonably well with the measured β_{mpp} values, as shown in Figure S4. Eq. (11) helps to make predictions about the FF of a solar cell just from the physical parameters of the active material.

2.4. Strategies to reduce FF losses

The initial step in reducing fill factor losses involves ensuring that the losses are accurately quantified, which requires the use of the correct metric. The higher limit for a solar cell without transport resistance, assuming external series resistance is negligible, is expressed through pFF . The fill factor tends towards this limit when β_{mpp} approaches 0. We find, similar to Green,³⁵ that for the values of the FF lying between 0.4 and 0.9, Eq. (8) can be approximated by a simple function $FF = v_{\text{oc}} / (v_{\text{oc}} + 4.37)$, where v_{oc} is defined as $eV_{\text{oc}} / (n_{\text{id}} + \beta_{\text{mpp}}) k_B T$. Using the same approximation for the pFF with $\beta = 0$ lets us estimate the ratio of the fill factors, i.e. the FF yield

$$\eta_{FF} = \frac{FF}{pFF} = \frac{eV_{\text{oc}} + 4.37n_{\text{id}}k_B T}{eV_{\text{oc}} + 4.37(n_{\text{id}} + \beta_{\text{mpp}})k_B T}. \quad (12)$$

Hence, this metric serves as a measure of the FF loss due to transport resistance. When transport resistance is absent, $\beta_{\text{mpp}} = 0$, and $\eta_{FF} = 1$. However, as transport resistance increases, η_{FF} tends to 0. In actual devices,

β is always greater than 0 but can be minimized. The prediction of FF loss based on Eq. (12) is depicted on Figure 5(a).

Fill factor losses are related to the collection efficiency, η_{col} , an important metric for assessing solar cell performance, quantified as the ratio of the collected current density j to the current density generated within the active layer of the solar cell j_{gen} . Voltage loss associated with transport resistance can be linked to the collection efficiency as

$$\Delta V_{\text{tr}} = -\frac{\alpha k_B T}{e} \cdot \eta_{\text{col}} (1 - \eta_{\text{col}})^{-n_{\text{id}}/n_{\sigma}} \quad (13)$$

Everything that does not get extracted recombines, therefore the complementary metric of η_{col} is the recombination efficiency, $\eta_{\text{rec}} = 1 - \eta_{\text{col}}$. Eq. (13) demonstrates that the voltage loss is in essence indeed competition between collection and recombination of charge carriers. Due to the relation between V_{mpp} and V_{oc} , the collection efficiency at MPP can simply be expressed as

$$\eta_{\text{col,mpp}} = \frac{v_{\text{oc}}}{v_{\text{oc}} + 1}, \quad (14)$$

where v_{oc} is again defined as $eV_{\text{oc}} / (n_{\text{id}} + \beta_{\text{mpp}}) k_B T$. The results are shown in Figure 5(b). Assuming that charge generation is field-independent, the internal quantum efficiency, $IQE \propto \eta_{\text{col}}$, is determined at MPP mainly by v_{oc} .

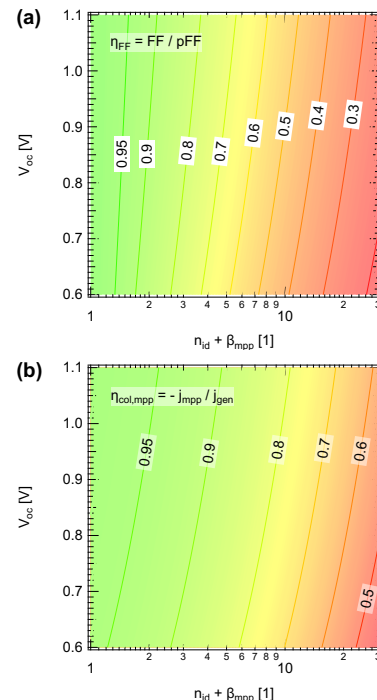


Figure 5. Calculated values of (a) the fill factor yield, η_{FF} , using Eq. (12) with $n_{\text{id}} = 1$, and (b) collection efficiency at the maximum power point, $\eta_{\text{col,mpp}}$, according to Eq. (14).

To mitigate FF losses and improve collection efficiency, it is essential to minimize the apparent ideality factor $n_{id} + \beta_{mpp}$, as evident from Figure 5. Various strategies can be employed for this purpose. One strategy involves reducing energetic disorder to attain $n_{id} = 1$ and decreasing trap density to mitigate the rate of trap-assisted recombination. The ratio n_{id}/n_{σ} affects both the additional term in Eq. (11), which increases β_{mpp} compared to α , as well as α itself, Eq. (7). This factor is dependent on the DOS, with the minimum value of 0.5, as described in Section S4. The prefactor j_{00}/σ_{00} plays a crucial role in reducing α , as demonstrated in Figure 3(e). Assuming the recombination rate constant k_r is treated within the reduced Langevin model, it is proportional to the mobility of the faster charge carrier.⁹ Conductivity, on the other hand, is limited by the slower charge carrier. Hence, achieving a lower ratio of μ_{fast}/μ_{slow} , along with a lower Langevin reduction factor, becomes essential for decreasing the prefactor, highlighting the importance of balanced charge carrier mobilities. Finally, transport resistance losses are linearly correlated with the thickness of the device, which makes them particularly relevant for industrial scale production of OSCs.

3. Conclusion

In conclusion, our research aimed to understand the factors influencing the fill factor of organic solar cells and find ways to improve the models related to transport resistance based on experimental data. We evaluated the transport resistance in various solution-processed organic solar cells, employing current-voltage and open-circuit voltage measurements. We presented a precise method for determining the effective conductivity at open circuit conditions, enabling the accurate evaluation of the figure of merit α , a measure of transport resistance at V_{oc} . The experimental observations revealed a strong correla-

tion between the fill factor and α , highlighting that the fill factor losses due to low conductivity in organic solar cells are a common issue and deserve more attention from the research community. Even in solar cells with comparatively low transport resistance ($\alpha \approx 1$), the fill factor loss is over 10% compared to the scenarios without transport resistance.

Based on the extensive experimental data, we have generalized the analytical model for transport resistance to account for the voltage dependence of recombination and transport, by including the corresponding ideality factors. We extended the diode equation accordingly, allowing for the evaluation of transport resistance at the maximum power point. The refined analytical model serves as a powerful tool for predicting the fill factor of a solar cell, based on its open-circuit voltage. Additionally, we introduced a metric for quantifying fill factor losses and collection efficiency at the maximum power point, along with strategies for mitigating these losses, thus enabling the development of more efficient optoelectronic devices.

Acknowledgements

We thank the Deutsche Forschungsgemeinschaft (DFG) for funding this work (Research Unit FOR 5387 POPULAR, project no. 461909888).

Competing interests

The authors declare no competing interests.

Data availability

The data supporting the findings of this study is available from the corresponding author upon reasonable request.

-
- [1] J. Wang, Y. Wang, P. Bi, Z. Chen, J. Qiao, J. Li, W. Wang, Z. Zheng, S. Zhang, X. Hao, and J. Hou, *Advanced Materials*, 2301583 (2023).
 - [2] M. Deng, X. Xu, Y. Duan, L. Yu, R. Li, and Q. Peng, *Advanced Materials* **35**, 2210760 (2023).
 - [3] W. Greenbank, N. Djeddaoui, E. Destouesse, J. Lamminaho, M. Prete, L. Boukezzi, T. Ebel, L. Bessissa, H.-G. Rubahn, V. Turkovic, and M. Madsen, *Energy Technology* **8**, 2000295 (2020).
 - [4] R. T. Grimm, P. Deb, D. J. Walwark Jr, C. Viets, and J. K. Grey, *The Journal of Physical Chemistry C* **124**, 16838 (2020).
 - [5] X. Du, T. Heumueller, W. Gruber, O. Almora, A. Classen, J. Qu, F. He, T. Unruh, N. Li, and C. J. Brabec, *Advanced Materials* **32**, 1908305 (2020).
 - [6] C. Liu, L. Lüer, V. M. L. Corre, K. Forberich, P. Weitz, T. Heumüller, X. Du, J. Wortmann, J. Zhang, J. Wagner, L. Ying, J. Hauch, N. Li, and C. J. Brabec, *Advanced Materials*, 2300259 (2023).
 - [7] C. Wöpke, C. Göhler, M. Saladina, X. Du, L. Nian, C. Greve, C. Zhu, K. M. Yallum, Y. J. Hofstetter, D. Becker-Koch, N. Li, T. Heumüller, I. Milekhin, D. R. T. Zahn, C. J. Brabec, N. Banerji, Y. Vaynzof, E. M. Herzig, R. C. I. MacKenzie, and C. Deibel, *Nature Communications* **13**, 3786 (2022).
 - [8] S. Schiefer, B. Zimmermann, and U. Würfel, *Journal of Applied Physics* **115** (2014).
 - [9] C. Göhler, A. Wagenpfahl, and C. Deibel, *Advanced Electronic Materials* **4**, 1700505 (2018).
 - [10] S. Shoaee, A. Armin, M. Stolterfoht, S. M. Hosseini,

- J. Kurpiers, and D. Neher, Solar RRL **3**, 1900184 (2019).
- [11] H. Bronstein, C. B. Nielsen, B. C. Schroeder, and I. McCulloch, Nature Reviews Chemistry **4**, 66 (2020).
- [12] M. Saladina, P. Simón Marqués, A. Markina, S. Karuthedath, C. Wöpke, C. Göhler, Y. Chen, M. Allain, P. Blanchard, C. Cabanetos, D. Andrienko, F. Laquai, J. Gorenflot, and C. Deibel, Advanced Functional Materials **31**, 2007479 (2021).
- [13] D. Cheyns, J. Poortmans, P. Heremans, C. Deibel, S. Verlaak, B. Rand, and J. Genoe, Physical Review B **77**, 165332 (2008).
- [14] F. F. Stelzl and U. Würfel, Physical Review B **86**, 075315 (2012).
- [15] T. Müller, B. E. Pieters, U. Rau, and T. Kirchartz, Journal of Applied Physics **113** (2013).
- [16] H. Mäckel and R. C. MacKenzie, Physical Review Applied **9**, 034020 (2018).
- [17] D. Bartesaghi, I. D. C. Pérez, J. Kniepert, S. Roland, M. Turbiez, D. Neher, and L. J. A. Koster, Nature Communications **6**, 7083 (2015).
- [18] U. Würfel, D. Neher, A. Spies, and S. Albrecht, Nature Communications **6**, 6951 (2015).
- [19] D. Neher, J. Kniepert, A. Elimelech, and L. J. A. Koster, Scientific Reports **6**, 24861 (2016).
- [20] P. Kaienburg, U. Rau, and T. Kirchartz, Physical Review Applied **6**, 024001 (2016).
- [21] B. Xiao, P. Calado, R. C. MacKenzie, T. Kirchartz, J. Yan, and J. Nelson, Physical Review Applied **14**, 024034 (2020).
- [22] N. Tokmoldin, J. Vollbrecht, S. M. Hosseini, B. Sun, L. Perdigón-Toro, H. Y. Woo, Y. Zou, D. Neher, and S. Shoaee, Advanced Energy Materials **11**, 2100804 (2021).
- [23] W. Yang, L. Ye, F. Yao, C. Jin, H. Ade, and H. Chen, Nano Research **12**, 777 (2019).
- [24] U. Rau, V. Huhn, and B. E. Pieters, Physical review applied **14**, 014046 (2020).
- [25] D. Grabowski, Z. Liu, G. Schöpe, U. Rau, and T. Kirchartz, Solar RRL **6**, 2200507 (2022).
- [26] M. List, J. Faisst, F. Heinz, and U. Würfel, Advanced Optical Materials **11**, 2300895 (2023).
- [27] M. A. Green, Solid State Electronics **24**, 788 (1981).
- [28] M. Saladina, C. Wöpke, C. Göhler, I. Ramirez, O. Gerdes, C. Liu, N. Li, T. Heumüller, C. J. Brabec, K. Walzer, M. Pfeiffer, and C. Deibel, Physical Review Letters **130**, 236403 (2023).
- [29] A. Foertig, J. Rauh, V. Dyakonov, and C. Deibel, Physical Review B **86**, 115302 (2012).
- [30] S. A. Hawks, F. Deledalle, J. Yao, D. G. Rebois, G. Li, J. Nelson, Y. Yang, T. Kirchartz, and J. R. Durrant, Advanced Energy Materials **3**, 1201 (2013).
- [31] A. Hofacker and D. Neher, Physical Review B **96**, 245204 (2017).
- [32] S. D. Baranovskii, physica status solidi (a) **215**, 1700676 (2018).
- [33] N. Tokmoldin, B. Sun, F. Moruzzi, A. Patterson, O. Alqahtani, R. Wang, B. A. Collins, I. McCulloch, L. Luüer, C. J. Brabec, D. Neher, and S. Shoaee, ACS Energy Letters **8**, 2552 (2023).
- [34] K. Taretto, M. Soldera, and M. Troviano, Progress in Photovoltaics: Research and Applications **21**, 1489 (2013).
- [35] M. A. Green, Solar Cells **7**, 337 (1982).
- [36] P. Würfel and U. Würfel, *Physics of solar cells: from basic principles to advanced concepts* (John Wiley & Sons, 2016).

Transport resistance strikes back: unveiling its impact on fill factor losses in organic solar cellsMaria Saladina¹ and Carsten Deibel¹¹*Institut für Physik, Technische Universität Chemnitz, 09126 Chemnitz, Germany***S1. EXPERIMENTAL METHODS****A. Device fabrication**

The materials PM6, PTB7, ITIC, o-IDTBR, and Y6 were acquired from 1-Material Inc., while PCBM was obtained from Solenne BV, and used as received. The solutions for the active layer blends were prepared in the following manner:

1. PM6:Y6, 1:1.2 w/w, 10 mg ml⁻¹ in chloroform with 0.5 vol.-% of 1-chloronaphthalene, stirred overnight at room temperature;
2. PM6:ITIC, 1:1 w/w, 10 mg ml⁻¹ in chloroform with 0.5 vol.-% of 1-chloronaphthalene, stirred overnight at room temperature;
3. PM6:o-IDTBR, 1:1 w/w, 10 mg ml⁻¹ in chloroform with 0.5 vol.-% of 1-chloronaphthalene, stirred overnight at room temperature;
4. PTB7:PCBM, 1:1.5 w/w, 25 mg ml⁻¹ in chlorobenzene with 3 vol.-% of DIO, stirred overnight at 60 °C.

Pre-patterned indium tin oxide (ITO)-coated glass substrates underwent cleaning in an ultrasonic bath with detergent, acetone, isopropanol, and deionized water. Subsequently, they were exposed to low-pressure oxygen plasma for 5 min. A 35 nm layer of poly(3,4-ethylenedioxythiophene) polystyrene sulfonate (PEDOT:PSS, Clevios AI 4083, Heraeus Deutschland GmbH & Co. KG) was spin-coated and annealed at 140 °C for 10 min. The active layers of nonfullerene acceptor solar cells was spin-coated in a nitrogen-filled glovebox from blend solution at 3000 r.p.m., while PTB7:PCBM blend was spin-coated at 600 r.p.m. PM6:ITIC and PM6:o-IDTBR were annealed at 100 °C for 10 min. The nonfullerene acceptor solar cells were finalized by depositing a 5 nm layer of bathocuproine (Ossila BV) and 100 nm of thermally evaporated Ag. For PTB7:PCBM, a 2 nm layer of Ca and 150 nm of Al were thermally evaporated on top of the active layer through a shadow mask with a base pressure below 10⁻⁶ mbar.

B. Current-voltage measurements

The samples were excited using a continuous wave laser Omicron LDM A350, operating at a wavelength of 515 nm. The laser's output power, alongside Thorlabs neutral density filters controlled by Standa motorized filter wheels, allowed for modulation of illumination intensity. Throughout the measurement, a silicon photodiode continuously monitored the illumination intensity. The current output was measured with a Keithley 2634b source measure unit. Throughout the experiment, the sample was maintained within a Linkam Scientific LTS420 cryostat. This cryostat ensured low temperatures via a constant flow of liquid nitrogen using a Linkam Scientific LNP96-S liquid nitrogen pump and Linkam Scientific T96-S temperature controller.

S2. GENERATION CURRENT DENSITY

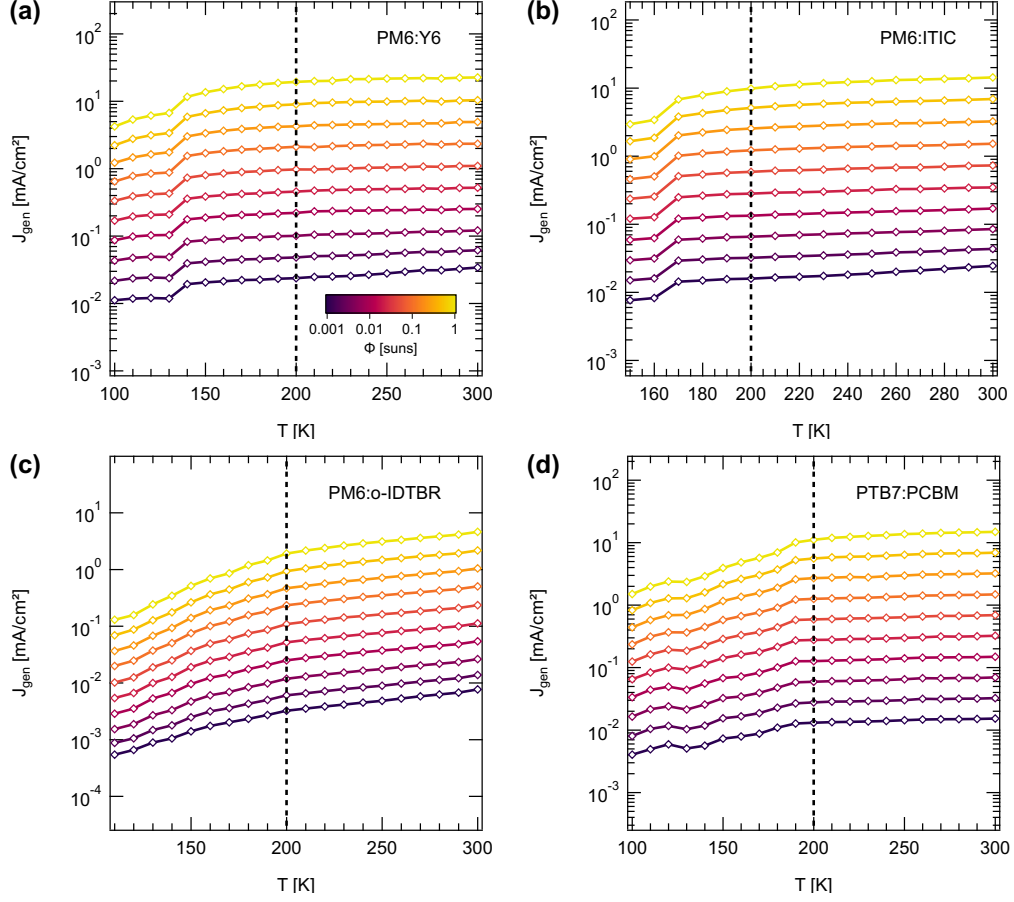


Figure S1. Generation current density j_{gen} as a function of temperature for (a) PM6:Y6, (b) PM6:ITIC, (c) PM6:o-IDTBR, and (d) PTB7:PCBM. Above 200 K, indicated by the dashed line, j_{gen} remains relatively constant. Data below 200 K was excluded from the analysis.

S3. APPARENT IDEALITY FACTOR AT V_{oc}

As described in the main text, apparent ideality factor is defined as $n_{\text{app}} = n_{\text{id}} + \beta$. At V_{oc} , parameter β is indeterminate because both $\Delta V_{\text{tr}} = jL/\sigma$ and $V_{\text{imp}} - V_{\text{oc}}$ are equal to 0. To evaluate β in the limit of $j \rightarrow 0$, we use L'Hopital's rule

$$\lim_{j \rightarrow 0} \beta = n_{\text{id}} \cdot \frac{d\Delta V_{\text{tr}}}{dj} \left[\frac{d(V_{\text{imp}} - V_{\text{oc}})}{dj} \right]^{-1}$$

The derivative of ΔV_{tr} is taken using Eq. (2) in the main text. Generally

$$\frac{d\Delta V_{\text{tr}}}{dj} = L \left(\sigma^{-1} + j \cdot \frac{d(\sigma^{-1})}{dj} \right). \quad (\text{S1})$$

The derivative of $V_{\text{imp}} - V_{\text{oc}}$ can be found using Eq. (1) in the main text, resulting in

$$\frac{d(V_{\text{imp}} - V_{\text{oc}})}{dj} = \frac{n_{\text{id}} k_B T}{e} \cdot \frac{1}{j + j_{\text{gen}}}.$$

At open circuit conditions $j = 0$, and $d\Delta V_{\text{tr}}/dj$ reduces to just one term, yielding $L/\sigma_{V_{\text{oc}}}$. The above equation is also simplified, leading to

$$\lim_{j \rightarrow 0} \beta = n_{\text{id}} \cdot \frac{L}{\sigma_{V_{\text{oc}}}} \cdot \left[\frac{n_{\text{id}} k_B T}{e} \cdot \frac{1}{j_{\text{gen}}} \right]^{-1} = \frac{eL}{k_B T} \cdot \frac{j_{\text{gen}}}{\sigma_{V_{\text{oc}}}} = \alpha.$$

This result yields $n_{\text{app}}|_{j=0} = n_{\text{id}} + \alpha$.

S4. THE RATIO OF THE IDEALITY FACTORS DESCRIBING THE VOLTAGE DEPENDENCE OF RECOMBINATION AND TRANSPORT

Earlier we have shown that recombination in PM6:Y6 is dominated by mobile charge carriers from the gaussian DOS recombining with the trapped ones from the power-law DOS.¹ The latter was approximated by an exponential DOS at a given energy, and therefore the apparent characteristic energy E_U was also energy dependent. The recombination ideality factor was analytically described as

$$n_{\text{id}}(E) = \frac{E_U(E) + k_B T}{2k_B T}.$$

The transport ideality factor, n_{σ} , which describes the voltage dependence of conductivity, can be derived using the multiple-trapping-and-release (MTR) model. Conductivity of electrons n and holes p is defines as

$$\begin{aligned} \sigma_n &= e\mu_{\text{eff},n} \cdot n = e\mu_{0,n} \cdot \theta_n \cdot n, \\ \sigma_p &= e\mu_{\text{eff},p} \cdot p = e\mu_{0,p} \cdot \theta_p \cdot p, \end{aligned}$$

where μ_{eff} denotes the effective (charge carrier density dependent) mobility, θ is the trapping factor, i.e. the share of mobile charge carriers, and μ_0 is their mobility.

At open circuit conditions the densities of electrons and holes are equal, and can be expressed analytically at a given quasi-Fermi level splitting as^{1,2}

$$n = p = n_i \cdot \exp\left(\frac{eV_{\text{oc}}}{E_U(E) + kT}\right),$$

where n_i is the intrinsic charge carrier concentration.

The trapping factor generally depends on the density of states. To simplify derivation we assign the the Gaussian DOS to electrons and the power-law DOS to holes. The results will have no loss of generality. With this assumption, the trapping factors are given by^{1,2}

$$\begin{aligned} \theta_n &= \exp\left(-\frac{s^2}{2(k_B T)^2}\right), \\ \theta_p &= N_0^{1-\lambda(E)} \cdot p^{\lambda(E)-1}. \end{aligned}$$

Here s is the standard deviation of the Gaussian distribution, N_0 is the total density of states, and $\lambda(E)$ is defined as $E_U(E)/k_B T$.

Using the above two equations, the conductivity of electrons and holes becomes

$$\begin{aligned} \sigma_n &= e\mu_{0,n} \cdot \exp\left(-\frac{s^2}{2(k_B T)^2}\right) \cdot n \propto \exp\left(\frac{eV_{\text{oc}}}{k_B T} \cdot \frac{k_B T}{E_U(E) + k_B T}\right), \\ \sigma_p &= e\mu_{0,p} \cdot N_0^{1-\lambda(E)} \cdot p^{\lambda(E)} \propto \exp\left(\frac{eV_{\text{oc}}}{k_B T} \cdot \frac{E_U(E)}{E_U(E) + k_B T}\right). \end{aligned}$$

It follows that depending on the density of states, the voltage dependence of conductivity is expressed differently. As already mentioned, recombination in PM6:Y6 is governed by mobile charge carriers from the Gaussian DOS. If transport resistance is dominated by the same mobile charge carrier, the ratio of the ideality factors is

$$\frac{n_{\text{id}}}{n_{\sigma}} = \frac{1}{2}.$$

However, if transport resistance is governed by the mobile charge carrier of the opposite type, then the ratio has different expression

$$\frac{n_{\text{id}}}{n_{\sigma}} = \frac{E_U(E)}{2k_B T} = n_{\text{id}} - \frac{1}{2}.$$

The difference between the ratios of the ideality factors helps to distinguish which density of states limits the fill factor. Only in the special case of $n_{\text{id}} = 1$ the latter equation yields the same result $1/2$, and the dominance can not be determined.

S5. THE RELATIONSHIP BETWEEN THE FIGURE OF MERIT α AND THE FILL FACTOR

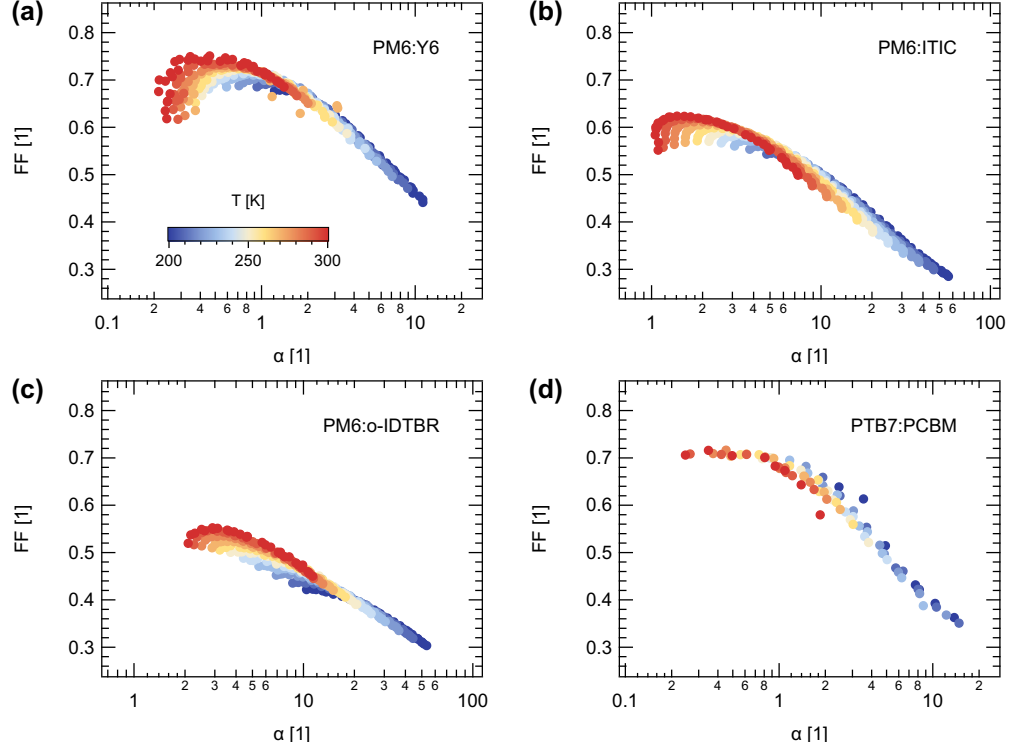


Figure S2. Fill factor as a function of α for (a) PM6:Y6, (b) PM6:ITIC, (c) PM6:o-IDTBR, and (d) PTB7:PCBM. The results validate the anticipated relationship between FF and $\ln \alpha$ as proposed by Neher et al.³

S6. ANALYTICAL APPROXIMATION FOR THE FILL FACTOR

The diode equation given by Eq. (3) in the main text, can be rewritten using the normalized voltage v_i ,⁴ as

$$j = j_{\text{gen}} (\exp(v_{\text{ext}} - v_{\text{oc}}) - 1), \quad \text{where} \quad v_i = \frac{eV_i}{n_{\text{app}} k_B T} \quad (\text{S2})$$

At the maximum power point, the derivative of the jV_{ext} product with respect to voltage is zero

$$0 = j + V_{\text{ext}} \cdot \frac{dj}{dV_{\text{ext}}} \approx j + v_{\text{ext}} \cdot \frac{dj}{dv_{\text{ext}}}.$$

The latter expression can be verified using the chain rule, and it holds if n_{app} changes little with voltage near the maximum power point. It leads to

$$\exp v_{\text{oc}} = \exp v_{\text{mpp}} \cdot (v_{\text{mpp}} + 1).$$

Using approximation of the Lambert W-function,⁵ one finds that

$$v_{\text{mpp}} \approx v_{\text{oc}} - \ln(v_{\text{oc}} + 1).$$

Applying this result to Eq. (S2) for the current density yields

$$j_{\text{mpp}} \approx j_{\text{gen}} \cdot \frac{v_{\text{oc}}}{v_{\text{oc}} + 1}.$$

Note that in the latter expression j_{mpp} is positive, therefore the minus sign is omitted. Finally, the fill factor is obtained using the last two equations, yielding Eq. (8) in the main text.⁶

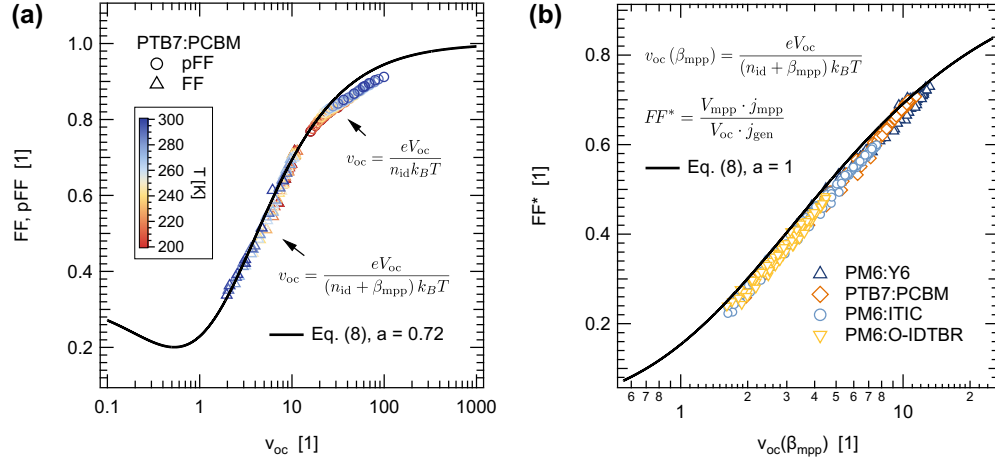


Figure S3. The fill factor approximation given by Eq. (8) is applied to (a) FF and pFF of a PTB7:PCBM solar cell. The pseudo-fill factor pFF represents the upper limit of FF obtained from the pseudo- $j(V)$ curve with zero transport resistance, therefore v_{oc} is determined by setting $\beta_{\text{mpp}} = 0$. In (b), FF^* is calculated using j_{gen} instead of j_{sc} . Eq. (8) approximates the data in (a) with $a = 0.72$, and in (b) with $a = 1$.

If the fill factor is calculated using j_{gen} instead of j_{sc} , here denoted as FF^* , parameter $a = 1$. We validate this approximation in Figure S3(b), where FF^* was obtained using j_{gen} , which was estimated from the current density at -0.5 V. Green found empirically that setting $a = 0.72$ greatly improves approximation of the fill factor.⁴ Indeed, for the real fill factor calculated using j_{sc} , we find that Eq. (8) with $a = 0.72$ works better, as shown in Figure S3(a) and Figure 4(c) in the main text.

S7. VOLTAGE LOSS DUE TO TRANSPORT RESISTANCE

Current density is expressed via implied voltage V_{imp} using Eq. (1) in the main text. Conductivity can be similarly expressed as a function of V_{imp}

$$\sigma(V_{\text{imp}}) = \sigma_{V_{\text{oc}}} \cdot \exp\left(\frac{eV_{\text{imp}} - eV_{\text{oc}}}{n_{\sigma}k_B T}\right).$$

Derivation of ΔV_{tr} is done in a similar way as in Neher et al.³ Substituting the above equation and Eq. (1) into Eq. (2) in the main text allows to obtain the general expression for the voltage loss due to transport resistance, ΔV_{tr}

$$\begin{aligned} \Delta V_{\text{tr}}(V_{\text{imp}}) &= \frac{L \cdot j(V_{\text{imp}})}{\sigma(V_{\text{imp}})} \\ &= \frac{k_B T}{e} \alpha \left[\exp\left(\left(1 - \frac{n_{\text{id}}}{n_{\sigma}}\right) \frac{eV_{\text{imp}} - eV_{\text{oc}}}{n_{\text{id}}k_B T}\right) - \exp\left(-\frac{n_{\text{id}}}{n_{\sigma}} \cdot \frac{eV_{\text{imp}} - eV_{\text{oc}}}{n_{\text{id}}k_B T}\right) \right]. \end{aligned} \quad (\text{S3})$$

A. ΔV_{tr} at open circuit conditions

Near the open circuit ΔV_{tr} can be approximated using the Taylor expansion

$$\Delta V_{\text{tr}}(V_{\text{imp}}) \approx (V_{\text{imp}} - V_{\text{oc}}) \cdot \left. \frac{d\Delta V_{\text{tr}}}{dV_{\text{imp}}} \right|_{V_{\text{imp}}=V_{\text{oc}}} = (V_{\text{imp}} - V_{\text{oc}}) \cdot \frac{\alpha}{n_{\text{id}}}.$$

Consequently, α is a good measure of the transport resistance at these conditions. Away from V_{oc} the exponential terms become sufficiently large, and the approximation deviates from the real value of ΔV_{tr} . The figure of merit α is not sufficient at the maximum power point to fully encompass ΔV_{tr} , and therefore β has to be used.

B. ΔV_{tr} at the maximum power point

Using Eqs. (1) and (3) in the main text, we can replace V_{imp} with V_{ext} in Eq. (S3). We get

$$\Delta V_{\text{tr}} = \frac{k_B T}{e} \alpha \left[\exp\left(\left(1 - \frac{n_{\text{id}}}{n_{\sigma}}\right) \frac{eV_{\text{ext}} - eV_{\text{oc}}}{(n_{\text{id}} + \beta)k_B T}\right) - \exp\left(-\frac{n_{\text{id}}}{n_{\sigma}} \cdot \frac{eV_{\text{ext}} - eV_{\text{oc}}}{(n_{\text{id}} + \beta)k_B T}\right) \right]$$

Or, in terms of the normalized voltage

$$\Delta V_{\text{tr}} = \frac{k_B T}{e} \alpha \left[\exp\left(\left(1 - \frac{n_{\text{id}}}{n_{\sigma}}\right) \cdot (v_{\text{ext}} - v_{\text{oc}})\right) - \exp\left(-\frac{n_{\text{id}}}{n_{\sigma}} \cdot (v_{\text{ext}} - v_{\text{oc}})\right) \right]$$

At the maximum power point, $v_{\text{ext}} = v_{\text{mpp}}$, and $v_{\text{mpp}} - v_{\text{oc}} \approx -\ln(v_{\text{oc}} + 1)$. With this approximation, the voltage loss due to transport resistance at the maximum power point becomes

$$\begin{aligned} \Delta V_{\text{tr}}|_{\text{mpp}} &\approx \frac{k_B T}{e} \alpha \left[\exp\left(\left(1 - \frac{n_{\text{id}}}{n_{\sigma}}\right) \cdot \ln\left(\frac{1}{v_{\text{oc}} + 1}\right)\right) - \exp\left(-\frac{n_{\text{id}}}{n_{\sigma}} \cdot \ln\left(\frac{1}{v_{\text{oc}} + 1}\right)\right) \right] \\ &= \frac{k_B T}{e} \alpha \left[(v_{\text{oc}} + 1)^{\left(\frac{n_{\text{id}}}{n_{\sigma}} - 1\right)} - (v_{\text{oc}} + 1)^{\frac{n_{\text{id}}}{n_{\sigma}}} \right] \\ &= -\frac{k_B T}{e} \alpha \cdot v_{\text{oc}} \cdot (v_{\text{oc}} + 1)^{\frac{n_{\text{id}}}{n_{\sigma}} - 1} \end{aligned}$$

Inserting this result into Eq. (4) in the main text yields Eq. (11) for β at the maximum power point. The result of the iteration using Eq. (11) is plotted in Figure S4.

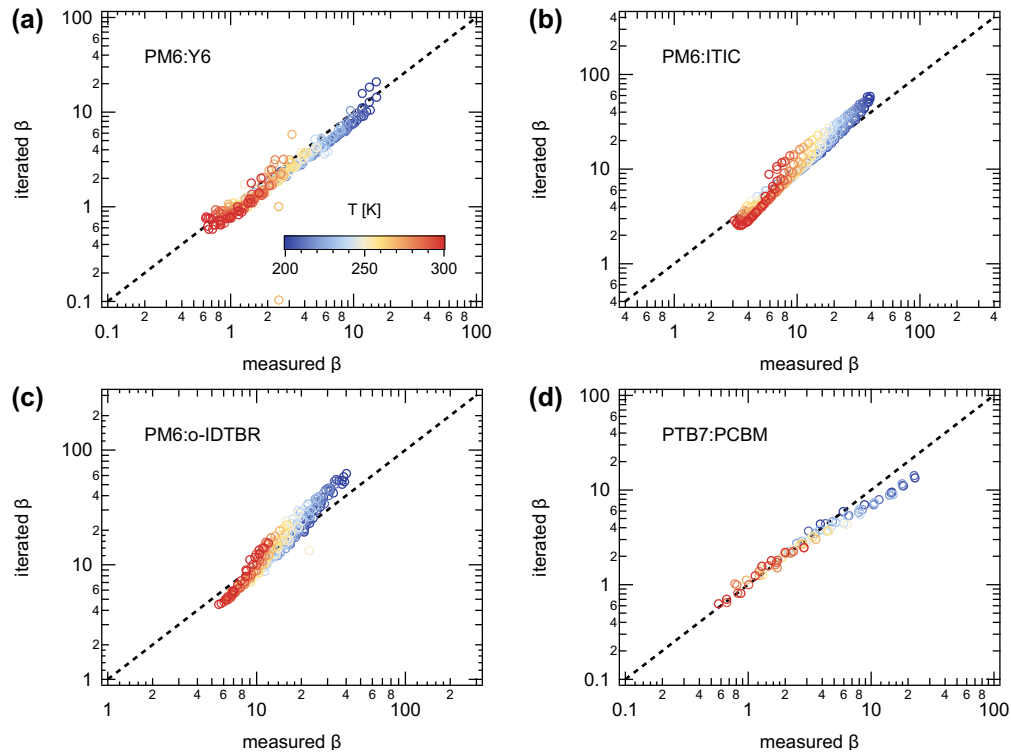


Figure S4. The parameter β at the maximum power point determined through iteration using Eq. (11) in the main text, and compared to measured β for (a) PM6:Y6, (b) PM6:ITIC, (c) PM6:o-IDTBR, and (d) PTB7:PCBM. The dashed line indicates the equality between the iterated and actual values.

-
- [1] M. Saladina, C. Wöpke, C. Göhler, I. Ramirez, O. Gerdes, C. Liu, N. Li, T. Heumüller, C. J. Brabec, K. Walzer, M. Pfeiffer, and C. Deibel, *Physical Review Letters* **130**, 236403 (2023).
 - [2] A. Hofacker and D. Neher, *Physical Review B* **96**, 245204 (2017).
 - [3] D. Neher, J. Kniepert, A. Elimelech, and L. J. A. Koster, *Scientific Reports* **6**, 24861 (2016).
 - [4] M. A. Green, *Solar Cells* **24**, 788 (1981).
 - [5] K. Taretto, M. Soldera, and M. Troviano, *Progress in Photovoltaics: Research and Applications* **21**, 1489 (2013).
 - [6] M. A. Green, *Solar Cells* **7**, 337 (1982).